Physics and Astronomy   College of Arts and Sciences

2009

Hubble Space Telescope Discovery of a z = 3.9 Multiply Imaged Galaxy Behind the Complex Cluster Lens WARPS J1415.1+36 at z = 1.026

Xiaosheng Huang
University of San Francisco, xhuang22@usfca.edu

T Morokuma

HK Fakhouri

G Aldering

R Amanullah

See next page for additional authors

Follow this and additional works at: http://repository.usfca.edu/phys

Part of the Astrophysics and Astronomy Commons, and the Physics Commons

Recommended Citation

Authors

Xiaosheng Huang, T Morokuma, HK Fakhouri, G Aldering, R Amanullah, K Barbary, M Brodwin, NV Connolly, KS Dawson, M Doi, L Faccioli, V Fadeyev, AS Fruchter, G Goldhaber, MD Gladders, JF Hennawi, Y Ihara, MJ Jee, M Kowalski, K Konishi, C Lidman, J Meyers, LA Moustakas, S Perlmutter, D Rubin, DJ Schlegel, AL Spadafora, N Suzuki, N Takanashi, and N Yasuda

HUBBLE SPACE TELESCOPE DISCOVERY OF A $z = 3.9$ MULTIPLY IMAGED GALAXY BEHIND THE COMPLEX CLUSTER LENS WARPS J1415.1+36 AT $z = 1.026$[*]

X. Huang[1], T. Morokuma[2,17], H. K. Fakhouri[1,3], G. Aldering[3], R. Amanullah[4], K. Barbary[1,3], M. Brodwin[5,18],
N. V. Connolly[6], K. S. Dawson[7], M. Doi[8], L. Faccioli[3], V. Fadeyev[9], A. S. Fruchter[10], G. Goldhaber[1,3],
M. D. Gladders[11], J. F. Hennawi[1], Y. Ihara[8,17], M. J. Jee[12], M. Kowalski[13], K. Konishi[14], C. Lidman[15], J. Meyers[1,3],
L. A. Moustakas[16], S. Perlmutter[1,3], D. Rubin[1,3], D. J. Schlegel[3], A. L. Spadafora[3], N. Suzuki[3], N. Takanashi[2],
AND N. Yasuda[14]

[1] Department of Physics, University of California Berkeley, Berkeley, CA 94720, USA; xhuang@lbl.gov
[2] National Astronomical Observatory of Japan, 2-21-1 Osawa, Mitaka, Tokyo 181-8588, Japan
[3] E. O. Lawrence Berkeley National Laboratory, 1 Cyclotron Road, Berkeley, CA 94720, USA
[4] Department of Physics, Stockholm University, Albanova University Center, S-106 91 Stockholm, Sweden
[5] Harvard-Smithsonian Center for Astrophysics, 60 Garden Street, Cambridge, MA 02138, USA
[6] Department of Physics, Hamilton College, Clinton, NY 13323, USA
[7] Department of Physics and Astronomy, University of Utah, Salt Lake City, UT 84112, USA
[8] Institute of Astronomy, Graduate School of Science, University of Tokyo 2-21-1 Osawa, Mitaka, Tokyo 181-0015, Japan
[9] Santa Cruz Institute for Particle Physics, University of California, Santa Cruz, CA 95064, USA
[10] Space Telescope Science Institute, 3700 San Martin Drive, Baltimore, MD 21218, USA
[11] Department of Astronomy and Astrophysics, The University of Chicago, 5640 S. Ellis Ave., Chicago, IL 60637, USA
[12] Department of Physics, University of California, Davis, One Shields Ave., Davis, CA 95616, USA
[13] Humboldt Universität Institut für Physik, Newtonstrasse 15, 12489 Berlin, Germany
[14] Institute for Cosmic Ray Research, University of Tokyo, 5-1-5, Kashiwanoha, Kashiwa, Chiba 277-8582, Japan
[15] Oskar Klein Center, Roslagstullsbacken 21, 106 91 Stockholm, Sweden
[16] Jet Propulsion Laboratory, California Institute of Technology, 4800 Oak Grove Dr., MS 169-327, Pasadena, CA 91109, USA

ABSTRACT

We report the discovery of a multiply lensed Lyα emitter at $z = 3.90$ behind the massive cluster WARPS J1415.1+3612 at $z = 1.026$. Images taken by the *Hubble Space Telescope* using the Advanced Camera for Surveys reveal a complex lensing system that produces a prominent, highly magnified arc and a triplet of smaller arcs grouped tightly around a spectroscopically confirmed cluster member. Spectroscopic observations using the Faint Object Camera and Spectrograph on *Subaru* confirm strong Lyα emission in the source galaxy and provide the redshifts for more than 21 cluster members with a velocity dispersion of 807 ± 185 km s^{-1}. Assuming a singular isothermal sphere profile, the mass within the Einstein ring ($7.13 \pm 0\farcs38$) corresponds to a central velocity dispersion of 686^{+15}_{-19} km s^{-1} for the cluster, consistent with the value estimated from cluster member redshifts. Our mass profile estimate from combining strong lensing and dynamical analyses is in good agreement with both X-ray and weak lensing results.

Key words: galaxies: clusters: general – galaxies: clusters: individual (WARPS J1415.1+36) – gravitational lensing

1. INTRODUCTION

Surveys like SpARCS (Wilson et al. 2008), SPT (Ruhl et al. 2004), the Red-Sequence Cluster Surveys (RCS, Gladders 2004 and RCS-2, Gladders & Yee 2005; Yee et al. 2007), and the IRAC Shallow Survey (Eisenhardt et al. 2008) will discover thousands of galaxy clusters out to redshifts beyond $z = 1$. These large surveys will be used to probe dark energy and the underlying cosmology through direct measurements of the evolution of the cluster mass function. To fully utilize these data, it will be essential to derive reliable mass estimates from the cluster properties measured in these surveys.

Great effort has been dedicated to the development of cluster mass-observable relations in targeted cluster observations. Sunyaev–Zel'dovich (SZ) and X-ray observations probe the hot ionized intracluster gas and have been used to derive masses (LaRoque et al. 2006; Allen et al. 2008) and scaling relations that tie mass to the observed SZ quantities (Bonamente et al. 2008). Hicks et al. (2006) derive scaling relations between observed X-ray properties and the optical richness of clusters while Evrard et al. (2008) model the relationship between the velocity dispersion of cluster galaxies and cluster mass. Weak lensing measurements have been used to calibrate optical richness measurements from a large sample of clusters from the Sloan Digital Sky Survey (Koester et al. 2007; Johnston et al. 2007) and to calibrate X-ray measurements through the mass–temperature relations (Hoekstra 2007; Bardeau et al. 2007; Bergé et al. 2008). Strong lensing measurements typically have much smaller errors compared with the other methods but are restricted to the central region of clusters and are rare. Nevertheless, strong lensing systems have been studied in small samples of clusters (Comerford et al. 2006; Hennawi et al. 2008).

Large cluster surveys out to $z \sim 1$ have the potential to constrain the dark energy equation of state (e.g., Voit 2005), provided that the mass-observable relations are well calibrated. Full exploitation of the more distant clusters requires deep space-based observations. As a result, mass-observable relations

---

have been studied in far fewer clusters at $z > 1$ relative to low-redshift clusters. In a 219-orbit program (Program number 10496, PI: Perlmutter) to search for supernovae (SNe) with the *Hubble Space Telescope* (*HST*), we observed 25 of the highest redshift galaxy clusters known at the time (Dawson et al. 2009). These images support a rich program of cluster studies including the calibration of mass proxies at $z > 1$. One particular cluster from this program, selected from the Wide Angle *ROSAT* Pointed Survey, WARPS J1415.1+3612 at $z = 1.026$ (Perlman et al. 2002), has already been studied in X-ray (Maughan et al. 2006; Allen et al. 2008) and SZ (Muchovej et al. 2007) observations. We now have deep images from the Advanced Camera for Surveys (ACS) and spectroscopy from the Faint Object Camera and Spectrograph (FOCAS: Kashikawa et al. 2002) on *Subaru* reveals a pronounced strong lensing arc of a source Lyα emitting galaxy at $z = 3.90$. The new data from this program combined with previous and ongoing measurements enable a multi-probe analysis of the cluster mass-observable relation for this high-redshift cluster.

Here, we present an analysis of the strong lensing and dynamical mass of WARPS J1415.1+3612. The Letter is organized as follows: we describe the observations and data in Section 2, mass estimates are derived and compared in Section 3, and the summary is found in Section 4. Throughout this Letter, we use AB magnitudes and assume a cosmology with $\Omega_M = 0.3$, $\Omega_\Lambda = 0.7$, and $h = 0.7$.

2. OBSERVATIONS

2.1. ACS Images

WARPS J1415.1+3612 was observed seven times with ACS from 2005 November through 2006 April for a total integration of 2425 s in the F775W filter and 9920 s in the F850LP filter, hereafter i_{775} and z_{850}. Individual exposures were co-added using MultiDrizzle (Fruchter & Hook 2002) at a resolution of $0\farcs05$ pixel^{-1}. We use 25.678 and 24.867 as zero points for i_{775} and z_{850}, respectively (Sirianni et al. 2005).

The deep ACS images revealed a complex strong lensing system near the cluster core. The composite color image from the i_{775} and z_{850} data is shown in Figure 1. The arc system consists of at least five images. The main arc (A) is $6\farcs75$ (54.4 kpc at the cluster redshift) from the center of the cluster, which we take to be the position of the brightest cluster galaxy (BCG). To the SW of the main arc, there is a triplet of arcs (B, C, and D) around a spectroscopically confirmed cluster member (no. 13). About $5''$ south of the triplet, there is a fifth arc (E). The total i_{775} isophotal magnitudes for the arcs A–E are 23.44, 25.75, 25.46, 25.13, and 25.62, respectively. We use the i_{775} magnitudes because they suffer less contamination than the z_{850} magnitudes from the much redder elliptical cluster members. The magnitudes for arcs B, C, and D are obtained after the lensing galaxy has been subtracted using the b-spline model of Bolton et al. (2006). These five images lie very close to an imaginary arc centered on the BCG that subtends slightly more than $90°$. The radius of the Einstein ring for the cluster potential is taken to be the average of the two circles mentioned in Figure 1, $7.13 \pm 0\farcs38$. The uncertainty in the radius is determined from the difference between the two circles and the average.

The *B*-band luminosity for this cluster is estimated by summing up light from all the galaxies within approximately 1 Mpc of the BCG and then subtracting a background estimated from fields without clusters within the GOODS fields. We apply a *K*-correction to transform z_{850} to rest-frame *B* magnitude.
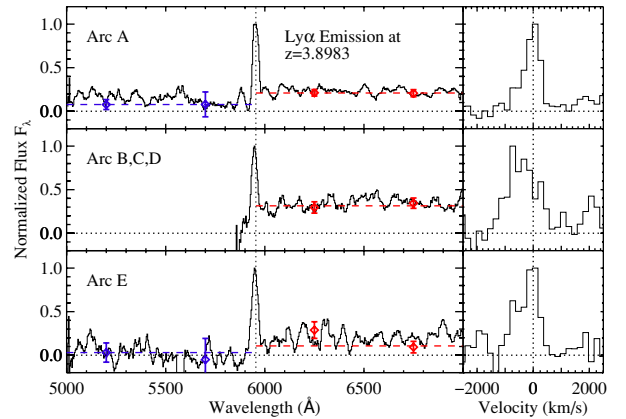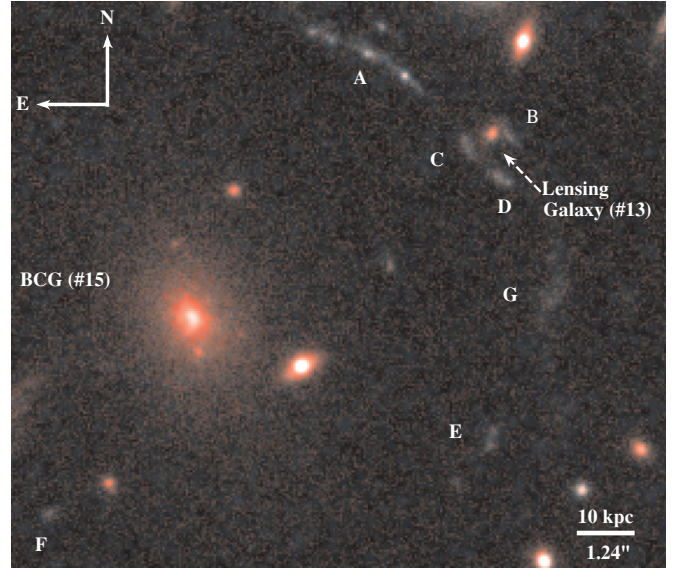
Figure 1. Top: central region of WARPS J1415.1+3612. Strong lensing arcs are labeled "A"–"E" and cluster galaxies of interest are labeled "no. 13" and "no. 15." The radius of the Einstein ring is taken to be the average of the radii of two imaginary circles (not shown), both centered on the BCG. The first circle with radius $6\farcs75$ passes through the center of arc A and the second, with radius $7\farcs51$, passes through cluster member no. 13 (the lensing galaxy). F and G are discussed in the text. Bottom: the panel on the left shows smoothed spectra of arc A; the triplet B, C, and D; and arc E. Zero flux is shown as the horizontal dotted lines. The diamonds with error bars are the average values of flux in 500 Å bins. The differences between the averages of the flux for wavelengths longer and shorter than the peak for arcs A and E (dashed lines) indicate the detection of discontinuity around the emission feature. The panel on the right shows the same spectra smoothed to the spectrograph resolution (FWHM = 600 km s^{-1}) and resampled by 200 km s^{-1} pixel^{-1} in the loglinear scale.

The total luminosity is determined to be $L_B = 2.92 \pm 0.88 \times 10^{12} \ L_{B\odot}$.

2.2. Subaru Spectroscopy

Spectroscopic observations were made with the FOCAS spectrograph on the *Subaru* telescope. SN candidates provided the primary targets for spectroscopic observations. The strong lensing arcs described in Section 2.1 and galaxies with $i_{775}-z_{850}$ color consistent with early-type galaxies at the cluster redshift provided secondary targets for multi-slit spectroscopy. We obtained spectra for a total of 138 objects and measured redshifts for 95 of them. Six masks were used, four with the 300R/SO58 grism and filter and two with the 300B/SY47 grism and filter. The total integration time is approximately 2 hr for each mask. Arcs B, C, and D were observed with the former

Table 1
Spectroscopic Redshifts

Object ID	R.A. (J2000)	Decl. (J2000)	z	Q
1	14:15:13.08	+36:12:25.4	1.0262 ± 0.0003	3
2	14:15:12.68	+36:12:59.6	1.0331 ± 0.0003	3
3	14:15:11.27	+36:14:35.7	1.033 ± 0.001	2
4	14:15:11.64	+36:11:37.8	1.028 ± 0.002	1
5	14:15:07.08	+36:14:15.6	1.0255 ± 0.0003	3
6	14:15:07.68	+36:13:06.3	1.025 ± 0.001	2
7	14:15:13.95	+36:12:37.8	1.017 ± 0.001	2
8	14:15:10.36	+36:11:31.2	1.0256 ± 0.0003	3
9	14:15:15.91	+36:12:58.9	1.0187 ± 0.0003	3
10	14:15:10.66	+36:11:39.8	1.028 ± 0.001	2
11	14:15:08.08	+36:12:21.0	1.0234 ± 0.0003	3
12	14:15:10.54	+36:12:09.9	1.0264 ± 0.0003	3
13[a]	14:15:10.59	+36:12:07.9	1.023 ± 0.002	1
14	14:15:10.19	+36:11:49.6	1.0313 ± 0.0003	3
15[a]	14:15:11.12	+36:12:04.0	1.0252 ± 0.0003	3
16	14:15:11.47	+36:12:22.8	1.018 ± 0.001	2
17	14:15:06.61	+36:12:18.0	1.033 ± 0.001	2
18	14:15:09.12	+36:13:09.1	1.0260 ± 0.0003	3
19	14:15:13.45	+36:12:56.9	1.035 ± 0.002	1
20	14:15:12.60	+36:11:09.7	1.023 ± 0.001	2
21	14:15:00.02	+36:13:02.8	1.011 ± 0.001	2
22	14:15:05.89	+36:13:03.1	1.025 ± 0.001	2
23	14:15:13.00	+36:13:07.0	1.0301 ± 0.0003	3
24	14:15:08.41	+36:13:04.6	1.035 ± 0.002	1
25	14:15:10.82	+36:10:33.0	1.023 ± 0.001	2
A	14:15:10.80	+36:12:09.1	3.8983 ± 0.0005	2
B–D[b]	14:15:10.57	+36:12:06.9	3.891 ± 0.002	2
E	14:15:10.58	+36:12:00.8	3.897 ± 0.001	2

Notes.
[a] Highlighted in Figure 1.
[b] Triplet unresolved in two-dimensional spectra.

setup, resulting in spectra that start at 5800 Å, while arc E was observed with the latter, resulting in spectra that cover a bluer wavelength range. Arc A was observed with both setups. The slit width is $0\farcs8$, corresponding to a spectral resolution of $R \sim 500$. Further details can be found in Morokuma et al. (2009).

Redshifts for cluster members were obtained by fitting a series of galaxy spectral eigenfunctions to the spectra weighted by the error spectra. For the majority of the spectra, the 3933 Å and 3968 Å Ca II H and K absorption lines were the dominant feature detected, along with the 4000 Å break and the [O II] emission line. Each redshift was assigned a quality flag Q, with $Q = 3$ for those with multiple strong features, $Q = 2$ for those with a single strong feature, and $Q = 1$ for those with only weakly detected features. Cluster members selected from the spectroscopically confirmed galaxies inside a radius of approximately 1 Mpc (or $\sim 2\farcm1$ at $z = 1.026$) are listed in Table 1. The redshift of the cluster is determined to be 1.026 from the average of the cluster member redshifts listed in the table. We calculate the cluster velocity dispersion from the 21 galaxies with $Q > 1$. Using the biweight scale estimator of Beers et al. (1990), we estimate $\sigma_v = 807 \pm 185$ km s^{-1} in the cluster rest frame. The measurement uncertainty is determined from bootstrap resampling of the data.

Spectra from each of the arc candidates (A–E) show significant emission around 5950 Å (Figure 1). The consistency in the observed emission wavelengths, surface brightness, color, and morphology of these five objects, and their arrangement around a circle centered on the BCG all strongly suggest that this is a multiply imaged system at $z > 1.026$. In this case, the line is

almost certainly Lyα at rest frame 1215.67 Å. The detection of discontinuity in flux for wavelengths bluer and redder than the emission feature in the spectra for arcs A and E lends support to the identification of this line with Lyα. Assuming this emission is due to Lyα, the redshifts of each arc are reported in Table 1. As indicated by the apparent discrepancy in redshifts, there is ~ 9 Å (or 453 km s^{-1} in the rest frame of the cluster, Figure 1) difference between the observed wavelengths of Lyα in arc A and in the triplet (arcs B, C, and D). It is three times the statistical error, which takes into account the spectral resolution. This difference is likely due to the placement of the arcs B, C, and D near the edges of the slit and contamination from the lensing galaxy (cluster member no. 13).

Preliminary spectroscopic results show that object F in Figure 1 is a possible counter arc of the same source galaxy. Object G in Figure 1 has the same color as arcs A–E and lies near the Einstein ring but spectroscopic data are inconclusive as to whether it has the same redshift as the confirmed arcs.

3. DISCUSSION

The total mass inside the Einstein ring of $r_E = 57.5 \pm 3.1$ kpc is $1.96^{+0.22}_{-0.20} \times 10^{13} M_\odot$ (e.g., Narayan & Bartelmann 1996). If we assume a singular isothermal sphere (SIS) profile for the central region of the cluster, this mass corresponds to a rest-frame velocity dispersion of 686^{+15}_{-19} km s^{-1}, consistent with the value estimated from cluster member redshifts. We can estimate the magnification factor for arc A by using $\mu = |1/(1 - r_E/r)|$ (e.g., Narayan & Bartelmann 1996) for the SIS profile, where r is the distance of the image from the lens center. If we take $r_E = 7\farcs13$ (or 57.5 kpc), $\mu \sim 18$ for arc A. This implies that the unmagnified i_{775} magnitude for arc A is ~ 26.6.

To get a qualitative estimate on the change in the derived strong lensing mass caused by relaxing our assumption of a spherically symmetric mass distribution, we construct elliptical Navarro–Frenk–White profile (NFW) models (Glose & Kneib 2002) with a critical curve that passes through at least part of arcs A and E and passes between arc C and the lensing galaxy (cluster member no. 13). The model with the largest ellipticity that still meets these requirements has an ellipticity of 0.1. The mass enclosed within its critical curve is $1.79 \times 10^{13} M_\odot$, within the errors of the spherical models.

The dynamical mass is estimated from the redshifts of the 21 cluster members with $Q > 1$ in Table 1 using the virial scaling relation from the simulations of Evrard et al. (2008),

$$\sigma_{DM}(M, z) = \sigma_{DM,15} \left(\frac{h(z)M_{200}}{10^{15} M_\odot} \right)^\alpha, \quad (1)$$

where $\sigma_{DM}(M, z)$ is the dark matter velocity dispersion, $h(z) = H(z)/100$ km s^{-1}, and M_{200} is the mass within r_{200} (the radius of a sphere where the mean density is 200 times the critical density at the redshift of the cluster). The constants $\sigma_{DM,15} = 1082.9 \pm 4.0$ km s^{-1} and $\alpha = 0.3361 \pm 0.0026$ are determined from the simulations of Evrard et al. (2008). Assuming that the velocity bias $b_v = \sigma_{v,gal}/\sigma_{DM} = 1$, we find $M_{200} = 3.33^{+2.83}_{-1.80} \times 10^{14} M_\odot$ and $r_{200} = 0.97 \pm 0.22$ Mpc. Thus, the mass to light ratio is $\sim 114 M_\odot/L_{B\odot}$. In Figure 2, we fit an NFW profile (Navarro et al. 1997) to the total cluster mass using the strong lensing and dynamical mass estimates. The model has a concentration parameter $c = 4.96^{+1.81}_{-1.03}$ and a core radius $r_s = 0.179^{+0.078}_{-0.055}$ Mpc, where uncertainties are computed via Monte Carlo simulation.
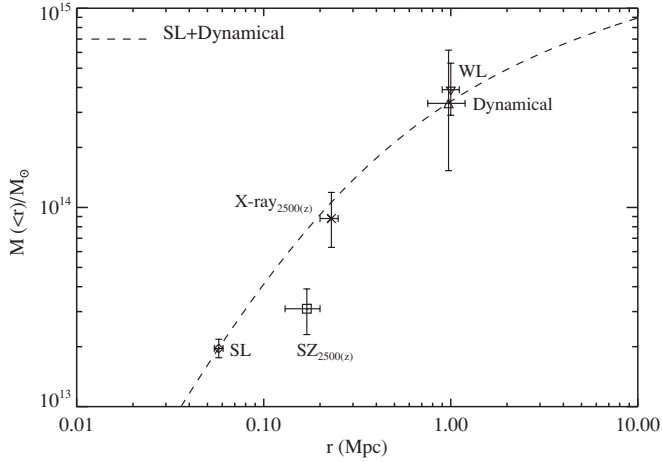
Figure 2. Comparison of different mass estimates for WARPS J1415+36. The strong lensing, weak lensing, and dynamical mass estimates presented in this work are labeled above. $M_{2500(z)}$ from the X-ray (Maughan et al. 2006) and SZ data (Muchovej et al. 2007) are also shown. The dashed line is an NFW profile fit to the strong lensing mass at $r_E = 0.0575$ Mpc and the dynamical mass at $r_{200} = 0.97$ Mpc ($c = 4.96^{+1.81}_{-1.03}$ and $r_s = 0.179^{+0.078}_{-0.055}$ Mpc).

For a simple test of the mass-observable relation in WARPS J1415.1+36, we compare our strong lensing and dynamical estimates and a model of the mass profile to an estimate of weak lensing mass, X-ray mass, and SZ mass in Figure 2. Using the same deep ACS images, M. J. Jee et al. (2009, in preparation) derive the weak lensing mass assuming an NFW profile with a mass–concentration relation from Bullock et al. (2001). The X-ray mass $M_{2500(z)}$ (Maughan et al. 2006) is determined from a best-fit two-dimensional elliptical β-model analyzed at $r_{2500(z)}$. The SZ value of $M_{2500(z)}$ is derived from a spherical, isothermal β-model fit to 30 GHz data from the SZ Array (Muchovej et al. 2007). In the X-ray and the SZ mass estimate, $\Delta(z)$ is a redshift-dependent density contrast as described in, e.g., Maughan et al. (2006). Both the weak lensing mass and the X-ray mass are consistent with our results. However, the SZ mass is lower than the prediction of our model by roughly a factor of 2. In Muchovej et al. (2007), it is noted that the SZ mass estimate is marginally lower than the X-ray value, likely due to low signal-to-noise ratio (S/N) in SZ measurements, uncertainties in the absolute calibration, and possible systematic errors from the model assumptions. Additional observations with the SZA at 30 GHz and 90 GHz should improve the constraints on the SZ mass estimate and shed light on the apparent discrepancy.

Using numerical simulations, Dolag et al. (2004) predict the dependence of the average halo concentration parameter on the cluster redshift and virial mass

$$c(M, z) = \frac{c_0}{1 + z} \left(\frac{M}{M_*} \right)^{\gamma}. \qquad (2)$$

Shaw et al. (2006) find the best-fit parameters to be $c_0 = 6.47 \pm 0.03$ and $\gamma = -0.12 \pm 0.03$ from N-body simulations. Here, M is the virial mass and $M_* = 11.0 \times 10^{14}$ $M_\odot$ (Shaw et al. 2006). If we assume the dynamical mass ($M_{200} = 3.33 \times 10^{14}$ $M_\odot$) to be the virial mass, Equation (2) predicts the average concentration to be $c = 3.70^{+0.62}_{-0.34}{}^{+1.9}_{-1.3}$, where the first set of errors is from the errors in the best-fit parameters (c_0 and γ) and the second set is from the scatter about the average (Bullock et al. 2001). Our concentration of $c = 4.96$ is higher than the predicted value of c but is well within its errors.

We now examine the strong lensing arcs B, C, and D around cluster member no. 13. The radius of the Einstein ring for the

lensing galaxy is estimated by the distance between the galaxy and arc C, $0\rlap{.}''65^{+0\rlap{.}''35}_{-0\rlap{.}''30}$. The upper and lower bounds are set by the distances from the lensing galaxy to arcs D and B, respectively. Assuming that the deflection angle due to the cluster potential does not vary appreciably for arcs B, C, and D, the mass enclosed within the Einstein radius is estimated to be $1.65^{+2.25}_{-1.17} \times 10^{11}$ $M_\odot$.

4. SUMMARY

The cluster WARPS J1415+36 at $z_{\rm lens} = 1.026$ is one of the most distant strong lensing clusters reported (Thompson et al. 2001; Gladders et al. 2003; Gilbank et al. 2008). Although the SZ mass estimate is not consistent with the rest of the data for this cluster, this work suggests that the mass-observable relations derived from numerical simulations and observations of strong lensing, weak lensing, dynamical mass, and X-ray mass still hold for clusters at redshifts at $z \sim 1$.

Recently Gilbank et al. (2008) report multi-probe mass estimates for the strong lensing cluster, RCS2319, at $z = 0.91$. Future surveys will soon reveal many new high-redshift, strong lensing systems and provide deep, multiwavelength images of these clusters. With the corresponding improvements in mass-observable relations in the decelerating regime, galaxy clusters will soon become an even more effective tool for cosmology.

REFERENCES

Allen, S. W., Rapetti, D. A., Schmidt, R. W., Ebeling, H., Morris, R. G., & Fabian, A. C. 2008, MNRAS, 383, 879
Bardeau, S., Soucail, G., Kneib, J.-P., Czoske, O., Ebeling, H., Hudelot, P., Smail, I., & Smith, G. P. 2007, A&A, 470, 449
Beers, T. C., Flynn, K., & Gebhardt, K. 1990, AJ, 100, 32
Bergé, J., et al. 2008, MNRAS, 385, 695
Bolton, A. S., Burles, S., Koopmans, L. V. E., Treu, T., & Moustakas, L. A. 2006, ApJ, 638, 703
Bonamente, M., Joy, M., LaRoque, S. J., Carlstrom, J. E., Nagai, D., & Marrone, D. P. 2008, ApJ, 675, 106
Bullock, J. S., Kolatt, T. S., Sigad, Y., Somerville, R. S., Kravtsov, A. V., Klypin, A. A., Primack, J. R., & Dekel, A. 2001, MNRAS, 321, 559
Comerford, J. M., Meneghetti, M., Bartelmann, M., & Schirmer, M. 2006, ApJ, 642, 39

Dawson, K. S., et al. 2009, AJ, 138, 1271
Dolag, K., Bartelmann, M., Perrotta, F., Baccigalupi, C., Moscardini, L., Meneghetti, M., & Tormen, G. 2004, A&A, 416, 853
Eisenhardt, P. R. M., et al. 2008, ApJ, 684, 905
Evrard, A. E., et al. 2008, ApJ, 672, 122
Fruchter, A. S., & Hook, R. N. 2002, PASP, 114, 144
Gilbank, D. G., Yee, H. K. C., Ellingson, E., Hicks, A. K., Gladders, M. D., Barrientos, L. F., & Keeney, B. 2008, ApJ, 677, L89
Gladders, M. D. 2004, in Clusters of Galaxies: Probes of Cosmological Structure and Galaxy Evolution, ed. J. S. Mulchaey, A. Dressler, & A. Oemler (Cambridge: Cambridge Univ. Press), 89
Gladders, M. D., Hoekstra, H., Yee, H. K. C., Hall, P. B., & Barrientos, L. F. 2003, ApJ, 593, 48
Gladders, M. D., & Yee, H. K. C. 2005, ApJS, 157, 1
Glose, G., & Kneib, J.-P. 2002, A&A, 390, 821
Hennawi, J. F., et al. 2008, AJ, 135, 664
Hicks, A. K., Ellingson, E., Hoekstra, H., & Yee, H. K. C. 2006, ApJ, 652, 232
Hoekstra, H. 2007, MNRAS, 379, 317
Johnston, D. E., et al. 2007, arXiv:0709.1159
Kashikawa, N., et al. 2002, PASJ, 54, 819
Koester, B. P., et al. 2007, ApJ, 660, 239

LaRoque, S. J., Bonamente, M., Carlstrom, J. E., Joy, M. K., Nagai, D., Reese, E. D., & Dawson, K. S. 2006, ApJ, 652, 917
Maughan, B. J., Jones, L. R., Ebeling, H., & Scharf, C. 2006, MNRAS, 365, 509
Morokuma, T., et al. 2009, PASJ, in press
Muchovej, S., et al. 2007, ApJ, 663, 708
Narayan, R., & Bartelmann, M. 1996, arXiv:astro-ph/9606001
Navarro, J. F., Frenk, C. S., & White, S. D. M. 1997, ApJ, 490, 493
Perlman, E. S., Horner, D. J., Jones, L. R., Scharf, C. A., Ebeling, H., Wegner, G., & Malkan, M. 2002, ApJS, 140, 265
Ruhl, J., et al. 2004, Proc. SPIE, 5498, 11
Shaw, L. D., Weller, J., Ostriker, J. P., & Bode, P. 2006, ApJ, 646, 815
Sirianni, M., et al. 2005, PASP, 117, 1049
Thompson, D., et al. 2001, A&A, 377, 778
Voit, G. M. 2005, Rev. Mod. Phys., 77, 207
Wilson, G., et al. 2008, in ASP Conf. Ser. 381, The Second Annual Spitzer Science Center Conf.: Infrared Diagnostics of Galaxy Evolution, ed. R.-R. Chary, H. I. Teplitz, & K. Sheth (San Francisco CA: ASP), 210
Yee, H. K. C., Gladders, M. D., Gilbank, D. G., Majumdar, S., Hoekstra, H., & Ellingson, E. 2007, in ASP Conf. Ser. 379, Cosmic Frontiers, ed. N. Metcalfe & T. Shanks (San Francisco, CA: ASP), 103